Article

In vivo imaging of vagal-induced myenteric plexus responses in gastrointestinal tract with an optical window

Longjie Jiang [1,2], Jie Yang [1,2], Xiujuan Gao [1,2], Jiangfeng Huang [1,2], Qian Liu [3] & Ling Fu [1,2,3,4,5] ✉

The vagus nerve (VN) extensively innervates the gastric enteric nervous system (ENS), but its influence on gastric ENS functionality and motility in vivo remains unclear due to technical challenges. Here we describe a method for stable, long-term observation of gastric ENS activity and muscle dynamics at cellular resolution, which can also be extended to intestinal applications. This method involves ENS-specific labeling and the implantation of an abdominal wall window for optical recording in male mice. In vivo calcium imaging reveals a linear relationship between vagal stimulation frequency and myenteric neuron activation in gastric antrum. Furthermore, the motility of gastric antrum is significantly enhanced and shows a positive correlation with the intensity and number of activated myenteric neurons. While vagal stimulation also activates proximal colonic myenteric neurons, this activation is not frequency-dependent and does not induce proximal colonic motility. The method and results provide important insights into VN-ENS interactions in vivo, advancing our understanding of gastrointestinal motility regulation.

The enteric nervous system (ENS), embedded within the gastro-intestinal (GI) wall, encompasses both the myenteric plexus (MP) and the submucosal plexus (SMP)[1]. The MP is crucial in regulating the GI tract's muscular layers—circular and longitudinal—which in turn orchestrate GI motility[2]. Moreover, the central nervous system (CNS) extends extrinsic neural inputs, notably through the vagus nerve, to finely tune GI motility[3]. As a critical element of the parasympathetic nervous system, the vagus nerve supplies essential innervation to the GI tract. Notably, the stomach exhibits the highest concentration of vagal afferent fibers, a density that diminishes progressively towards the colon[4]. The vagus nerve is instrumental in monitoring gastric status and modulating its motility. In contrast, the extrinsic regulation of colonic motility primarily relies on the sympathetic and sacral para-sympathetic nerves[5–7]. However, in vivo recording of the ENS activity and GI muscular movements presents significant challenges, including

spontaneous GI movements and the absence of a stable surface for affixing recording apparatus[8]. Consequently, there is a limited understanding of the real-time effects of the vagus nerve on the gastric ENS in live animals.

Intravital microscopy, achieved by the surgical implantation of an optical window, allows for long-term, in vivo imaging of multiple tissues and organs[9], including the skin[10], brain[11], spinal cord[12], small intestine[8], colon[13], lung[14], liver[15], embryos[16], among others. This method enables the monitoring of the activity of ENS in the mouse's small intestine and colon[8,13]. However, it is primarily used for researching the lower GI tract, which has a lower density of vagal innervation than the upper GI tract[17]. Nevertheless, to date, there is no stabilized, long-term, and cellular-resolution in vivo imaging approach specifically designed for gastric ENS in mice. This is due to the ana-tomical position of the stomach below the rib cage and partially

[1]Britton Chance Center for Biomedical Photonics, Wuhan National Laboratory for Optoelectronics, Huazhong University of Science and Technology, Wuhan, Hubei, China. [2]MoE Key Laboratory for Biomedical Photonics, Huazhong University of Science and Technology, Wuhan, Hubei, China. [3]School of Biomedical Engineering, Hainan University, Haikou, Hainan, China. [4]School of Physics and Optoelectronics Engineering, Hainan University, Haikou, Hainan, China. [5]Advanced Biomedical Imaging Facility, Huazhong University of Science and Technology, Wuhan, Hubei, China. ✉e-mail: lfu@mail.hust.edu.cn

covered by the liver[18], the high variability in stomach volume, and the motion artifacts caused by gastric peristalsis, cardiac pulsations, and respiratory movements[19]. These factors present significant challenges to in vivo investigations of the dynamics of the gastric ENS and its complex interactions with the vagus nerve. This highlights a critical area for future research advancements.

In this study, we present a pioneering method for in vivo imaging of gastric and colonic MP, which involves designing an optical window, its surgical implantation, and specifically labeling ENS. This approach guarantees the mice's long-term viability post-surgery and mitigates tissue displacement during live imaging via an external stabilizing fixture. Marking a significant advancement, we have successfully attained stable, long-term, and cellular-resolution in vivo imaging of the stomach and colon in mice. The standardized design of the optical window, coupled with uniform implantation procedures and ENS labeling, greatly enhances the in vivo investigation of the ENS across the GI tract. Using this technique. we observed the influence of vagal stimulation on the activity of myenteric neurons within both the stomach and colon, in vivo, through confocal calcium imaging of gastric and colonic MP. This exploration also extended to the structural and functional relationships between the vagus nerve and ENS in vivo. The optical window implementation has allowed for the first in vivo documentation of the gastric ENS, expanding ENS research from the lower to the upper gastrointestinal tract. Our method enables stable and reproducible examination of the ENS, mirroring in vivo imaging strategies used for the CNS. This capability is critical for capturing the impact of external neural inputs, such as the vagus nerve, on the ENS dynamics. Furthermore, the window's stability is instrumental for effectively documenting GI muscular movements triggered by external stimuli. The technique developed in this research is a valuable tool for exploring the ENS and understanding the modulation of ENS dynamics and gastric motility by the vagus nerve in real-time.

Results

In vivo imaging in the mouse stomach

To achieve in vivo stable imaging of the mouse stomach, we developed an experimental procedure and a confocal imaging system (Fig. 1a and **Online Methods**). The experimental procedure involves three steps: labeling of ENS in the wild-type mouse, then an optical window implanted above the stomach, and in vivo optical recording of the stomach[14]. Recombinant adeno-associated viruses (rAAV) are frequently utilized to specifically label the nervous system in vivo, enabling the study of neuronal activity and dynamics in real-time[20,21]. Injection of rAAV into GI wall allows for more precise, efficient, and targeted labeling of ENS than intravenous injection into the tail vein[20] (see Supplementary Fig. 1). Injecting directly into the wall of GI tract is more challenging than injecting into the brain due to the lack of the support in the GI tract compared to the skull. Additionally, the wall of GI tract is thin in mice. To prevent penetration of the GI wall, it is necessary to sharpen the tip of the injection glass tube (about 35 µm outside diameter) to less than 30° (see Supplementary Fig. 2). To avoid affecting digestive function inactivation at the injection site, injections must avoid blood vessels in the GI tract wall and not penetrate into the mucosal layer (see **Online Methods**). Our investigation of direct injection of rAAV into the GI wall (the muscle layer) successfully labeled neurons and glial cells within the ENS (see Supplementary Fig. 2). The study indicates that the injection of rAAV into the GI wall to label ENS, combined with optical windows, can effectively and accurately record the structure and function of ENS in vivo.

Previous studies have demonstrated that confocal imaging can penetrate from the serosal layer of the intestine to the MP[22]. In vivo imaging confirmed that gastric MP, when labeled with rAAV-hSyn-EGFP, can also be observed using confocal imaging (see Supplementary Fig. 3 and Supplementary Movie 1). A common image acquisition rate for recording neuronal activity in the ENS is 0.5–10 frames per second (fps)[23–26]. The risetimes and duration of calcium transients in gastric myenteric neurons were compared at image acquisition speeds of 2 fps and 20 fps in vivo, where neuronal activity is induced by gastric electrical stimulation (GES). The results showed no significant difference in risetimes (2 fps, 1.3 ± 0.2 seconds; 20 fps, 1.6 ± 0.1 seconds, $p = 0.09$) and duration (2 fps, 8.5 ± 0.6 seconds; 20 fps, 8.3 ± 0.6 seconds, $p = 0.56$) of calcium transients between the two acquisition speeds (see Supplementary Fig. 4). Therefore, the acquisition rate of the confocal imaging system for ENS recording is set at 2 fps. The imaging system's excitation light sources are 488 nm and 561 nm, allowing for simultaneous imaging of MP and vasculature, as well as neurons and glial cells in the stomach (see Supplementary Fig. 3).

Design of an optical window with the fixturing platform

Non-invasive fluorescence imaging using Red-to-NIR fluorescent probes has an excellent biocompatibility and stability and allows observation of gastric motility, but not ENS activity[27]. Intravital imaging has been utilized for imaging intestinal ENS at a cellular-resolution[13,28] but not the gastric ENS. For the first time, we have engineered an optical window designed for cell-resolution imaging of the stomach in live mice. The window consists of a window groove and two scaffolds, all made from titanium alloy for smoothness and biocompatibility, with a total weight of approximately 0.7 g (Fig. 1b and see Supplementary Fig. 5). The window groove includes three grooves. The groove 1 is designed to fit with a cover glass of 12 mm diameter and uses a circlip to secure the glass cover for easy replacement. The groove 2 is implanted in the muscle and skin layers and fixed with sutures. The groove 3 convolutes into the gastric scaffold providing necessary support (Fig. 1c). The gastric scaffold is devised for easy passage from the lesser curvature of the stomach to the base (Fig. 1d, e), providing support for the gastric antrum at the window and would not affect the digestive movement of the stomach (see Supplementary Fig. 6). To ensure stable imaging, we developed an external fixation platform that minimizes tissue movement during imaging sessions (Fig. 1h, see Supplementary 7 and Supplementary Movie 2). Furthermore, the design of the intestinal scaffold enables easy replacement, thereby extending imaging capabilities to the intestine (Fig. 1i–k). The scaffold and fixation platform configurations are detailed in supplementary Fig. 5.

Surgical procedures for implanting the gastric window ensure prolonged survival of mice

We developed a protocol (Fig. 1f, see Supplementary Fig. 6) for implanting an optical window in the stomach without impairing its digestive function. The method for implanting the window groove into the adjacent abdominal wall refers to the description by previous studies[29]. It is important to note that part of the fixed window groove is placed on the left ribs to prevent lateral displacement of the stomach during subsequent use of the gastric scaffold. After implanting the window groove, the gastric scaffold is guided through the window to the underside of the gastric antrum (the supine view of a mouse), providing structural support to the antrum (see Supplementary Movie 3). It is crucial to avoid damaging the pancreas to prevent any negative impact on the survival of mice. Postoperatively, mice are treated with wound disinfection and anti-inflammatory medication. If the procedure is performed correctly, this window can ensure that the mouse's movement and digestive function is almost unaffected (see Supplementary Movie 4). Additionally, it allows for observation of the same part of the stomach for up to 14 days (Fig. 1g), without causing gastric injury (see Supplementary Fig. 6). The maximum recorded survival time for mice is 31 days because the windows fell out. If the coverslip is left in contact with the stomach for more than 6 days, a thin layer of tissue will grow at the contact point, which can affect observation[16]. This issue can be resolved by replacing the coverslip before imaging.
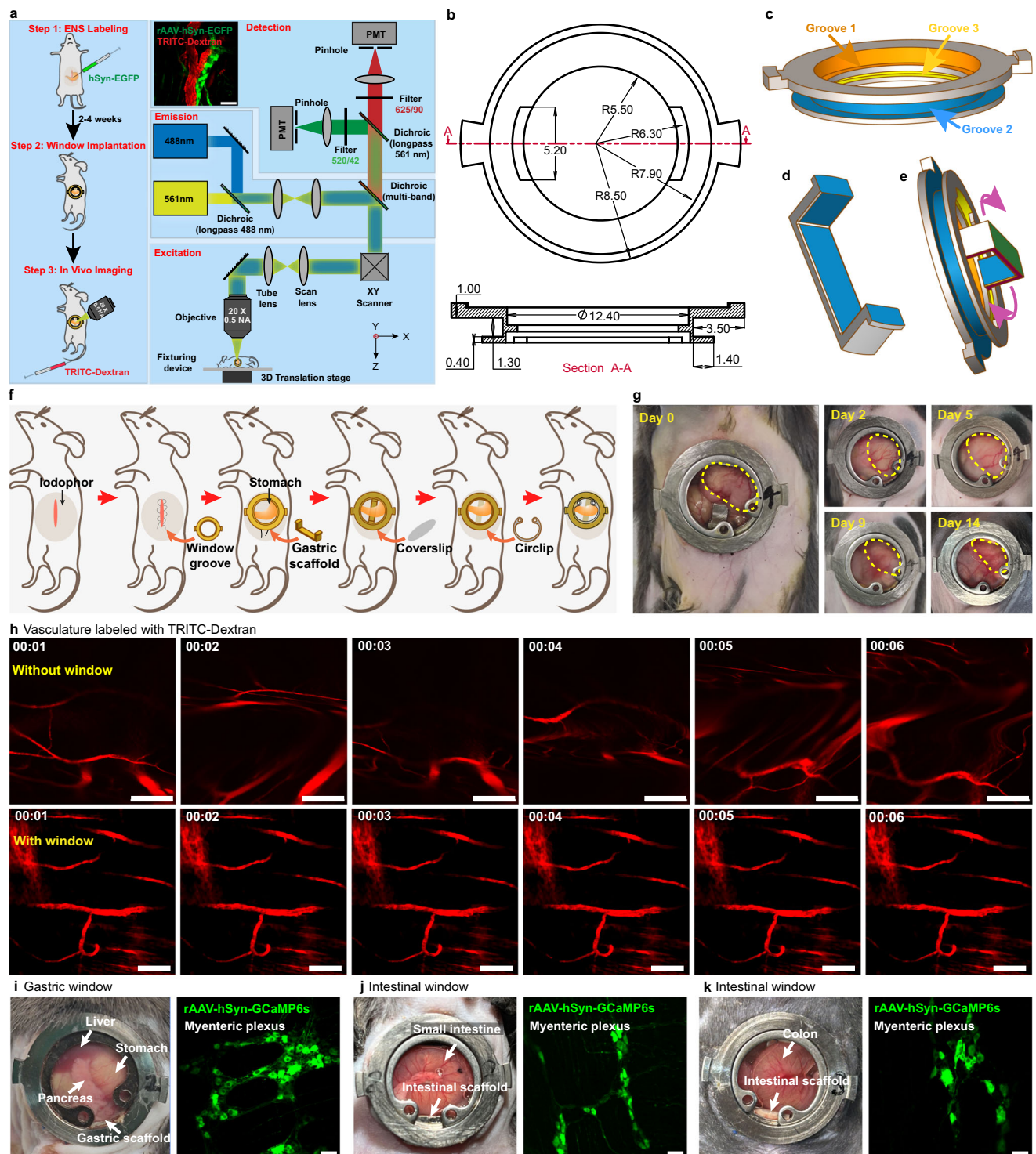
Fig. 1 | Intravital imaging of mouse stomach with an optical window. a Left, Schematic illustration of the steps for in vivo imaging of mouse stomach, with experimental timeline. Right, dual-channel confocal in vivo imaging of gastric MP and blood vessels, using a 488 nm laser, with detection centered at 520 nm and a 561 nm laser, with detection centered at 625 nm. The inset shows an example of a confocal image of EGFP expression (MP) and dextran labeling (vasculature). Scale bar is 100 μm. **b**–**e** Illustration of (**b**) the top view and side view of the gastric window, all dimensions are listed in millimeters. (**c**, **d**) The titanium optical window and gastric scaffold, (**e**) 3D view of the window with gastric scaffold is used for in vivo imaging of mouse stomach. **f** Overview of the surgical protocol. **g** Gastric window implanted in a mouse for up to 14 days, day 0 refers to the day of surgical implantation, and yellow dashed circles show the stomach. **h** Representative images of the blood vessels (TRITC-Dextran, red) of mouse stomach within 6 seconds without gastric window and with window. All scale bars are 100 μm. **i**–**k** Optical window used for the (**i**) stomach, (**j**) small intestine and (**k**) colon. The typical structure of rAAV-hSyn-GCaMP6s-labeled gastric, small intestinal, and colonic myenteric neurons (green) is also shown. All scale bars are 50 μm.
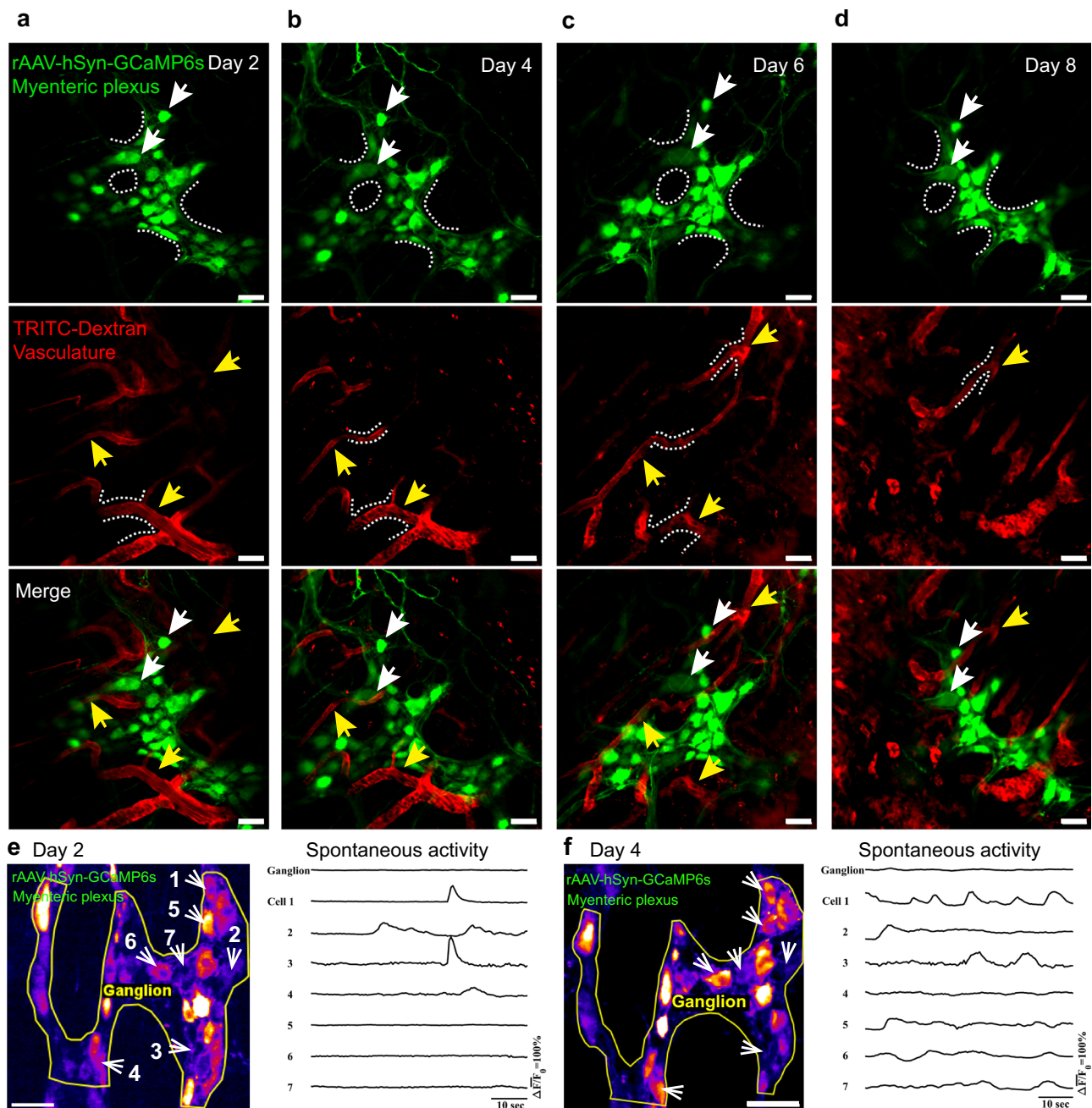
Fig. 2 | Chronic confocal imaging of gastric MP within the window.
a–**d** Representative single channel and merge confocal images of stomach in the same position on days 3, 5, 7, and 9 after window implantation (day 0). Neurons (white arrows) of MP are labeled with rAAV-hSyn-EGFP (green), and vasculature (yellow arrows) is labeled with TRITC-Dextran (red) in C57BL/6J mice. **e**–**f** Spontaneous calcium activity recordings from the same gastric neurons (rAAV-hSyn-GCaMP6s labeling) at different times (recordings on day 2 and day 4). The yellow line indicates a ganglion of the myenteric plexus, and the white arrow indicates a nerve cell. All scale bars are 50 μm.

Long-term and stable recording of gastric MP

We performed confocal imaging to observe the stomach in vivo through the implanted optical window in C57BL/6J mice. During the imaging sessions, the mice were kept under respiratory anesthesia. We were able to simultaneously visualize neurons of the MP labeled with rAAV-hSyn-EGFP (green) and the vasculature marked by TRITC-Dextran (red) within the same optical section using a dual-channel confocal imaging system. Imaging sessions were conducted on days 2, 4, 6, and 8 post-window implantation (with day 0 being the day of implantation), allowing one day of recovery for the mice after each session (Fig. 2a–d). Additionally, we successfully recorded the spontaneous calcium activity of the same MP neurons labeled

with GCaMP6s on days 2 and 4 (Fig. 2e, f and see Supplementary Movie 5, 6). The results demonstrate that the window can maintain the same position of the stomach for a long time. Consequently, this approach allows for the long-term stable imaging of gastric MP at a fixed location.

The vagus nerve innervation of gastric myenteric plexus and regulation of gastric motility

Studies investigating the role of the vagus nerve in regulating gastric motility have highlighted its direct connection to gastric MP[30], yet the underlying mechanisms remain largely unexplored. Utilizing cervical vagus nerve stimulation (VNS) at frequencies of 20 and 30 Hz, we
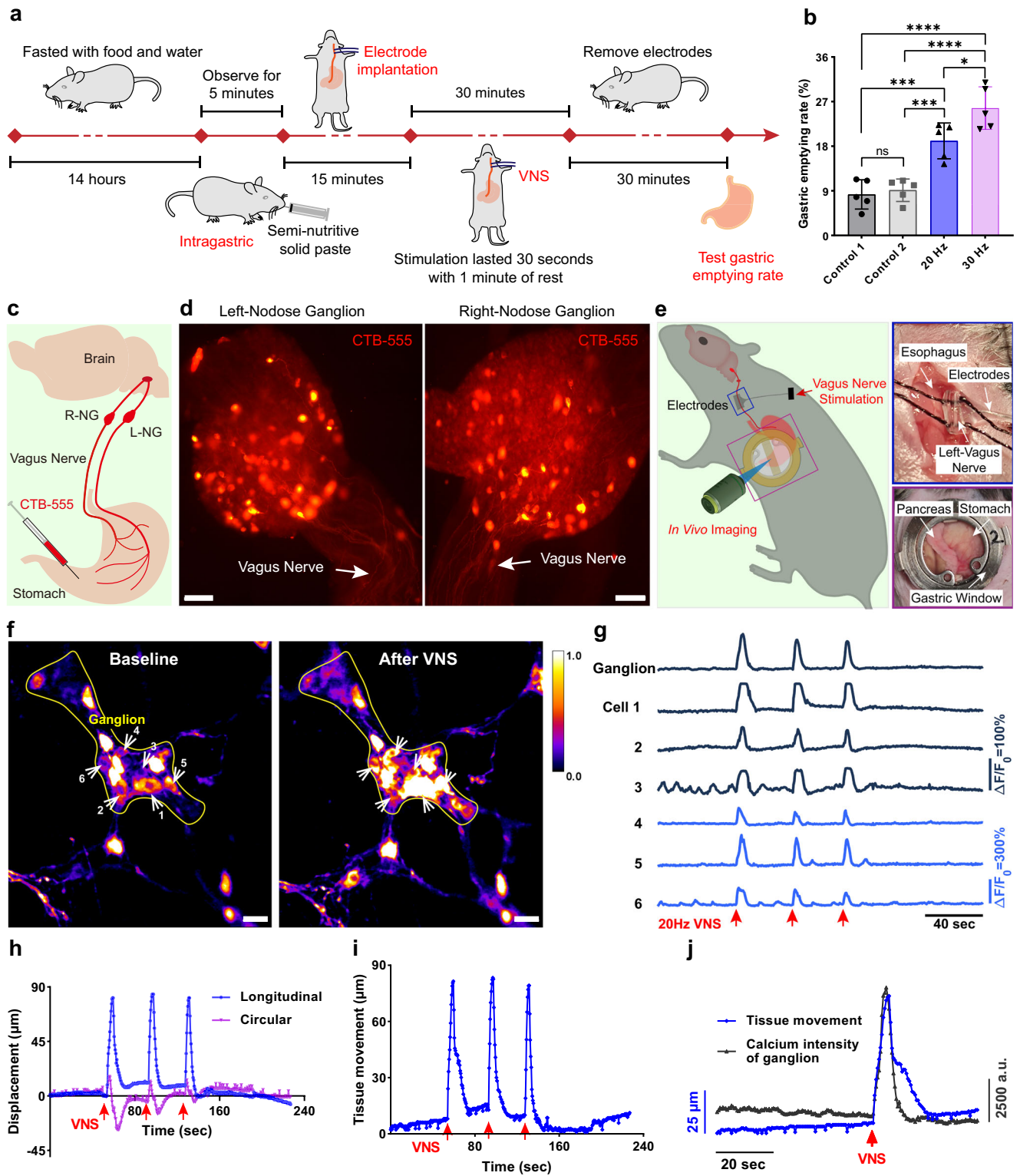
assessed its impact on gastric emptying in C57BL/6J mice through gastric gavage[31], revealing a significant ($p < 0.05$, $n = 5$ mice per group) enhancement in emptying rates (Fig. 3a, b and see Supplementary table 1). The robust stability of our implanted optical windows facilitated in vivo observations of gastric MP responses and tissue movement post-VNS (Fig. 1h and see Supplementary Fig. 8). The nerve fibers originating in the nodose ganglion supply the gastrointestinal organs[32]. To delineate the vagal neural pathways involved, we employed cholera toxin B subunit 555 (CTB-555) to retrogradely trace vagal fibers and neurons innervating the stomach (Fig. 3c). Both right

and left vagal nodose ganglia exhibited significant labeling, affirming a direct vagal neural linkage to the stomach (Fig. 3d), consistent with prior studies[33]. VNS, typically applied to the left vagus nerve at a range of 1–30 Hz[34,35], was conducted following the establishment of optical windows post-21 days of viral expression (rAAV-hSyn-GCaMP6s) and prior electrode implantation for VNS at the left esophagus (Fig. 3e). Subsequent stimulation led to notable alterations in calcium fluorescence intensity within myenteric neurons, indicative of neuronal activation (Fig. 3f, g and see Supplementary Movie 7). This stimulation, applied thrice at 20 Hz with intervals of approximately 30 seconds,

Fig. 3 | In vivo calcium imaging of the gastric myenteric plexus in response to VNS. a Steps for the gastric emptying rate test in C57BL/6J mice. **b** VNS significantly increases the rate of gastric emptying. Control 1 refers to the group of mice without implanted electrodes and Control 2 refers to the group of mice implanted with electrodes but no VNS ($n = 5$ mice per group). Control 1 vs Control 2, $p = 0.6262$; Control 1 vs 20 Hz, $p = 0.0009$; Control 1 vs 30 Hz, $p < 0.0001$; Control 2 vs 20 Hz, p = 0.0008; Control 2 vs 30 Hz, $p < 0.0001$; 20 Hz vs 30 Hz, $p = 0.0299$. ns: $p > 0.05$, *$p < 0.05$, ***$p < 0.001$, ****$p < 0.0001$, unpaired student t-test (two-tailed). **c** Cartoon depiction of a strategy for tracing the vagus nerves from the stomach. **d** Native fluorescence whole-map analysis of left- and right- ganglion and vagus nerves (white arrow) after gastric infection with CTB-555 in C57BL/6J mice. All scale bars are 200 μm. **e** Schematic of in vivo imaging of mouse stomach. The blue box shows a detail of electrode implantation for left VNS and the purple box shows a detailed view of the gastric window during imaging. **f** Frames were captured from in vivo confocal imaging of myenteric neurons expressing GCaMP6s during 20 Hz VNS. All scale bars are 50 μm. **g** Changes in calcium intensity from (**f**) ganglia and cells (white arrow) in response to 20 Hz VNS (red arrow, 3 times). The longitudinal coordinates of the curves for ganglia and cells 1, 2, and 3 are $\Delta F/F_0 = 100\%$ and cells 4, 5, and 6 are $\Delta F/F_0 = 300\%$. **h** Myenteric ganglia displacement (blue, longitudinal muscle axis; purple, circular muscle axis) to 20 Hz VNS (3 times). **i** Tissue movement to 20 Hz VNS of the stomach. **j** Calcium intensity traces of responsive myenteric ganglia (dark red) and resulting tissue movement (dark blue) to 20 Hz VNS (red arrow) of the stomach. All data are mean ± s.e.m.

---

correlated with significant shifts in calcium intensity across all regions of interest (ROI). Gastric tissue displacement in the x- and y- axes was directly correlated with circular and longitudinal muscle contraction[36]. We decomposed the movement of ganglia (ROI) into x and y directions after VNS (Fig. 3h), tissue movement equal to the square root of the sum of the squares of x and y coordinates (Fig. 3i). Analysis of gastric tissue movement, revealing a near-simultaneous occurrence of calcium intensity changes in ganglia with tissue movement (Fig. 3j). Our findings highlight the real-time interaction between the vagus nerve and the gastric MP, in which the vagus nerve activates myenteric neurons, subsequently inducing gastric tissue motility and enhancing gastric peristalsis. These data suggest that this optical window can be used for stable real-time observation of the activity of the MP as well as the gastric tissue motility induced by vagal activation.

Comparing the activity evoked by different frequencies of VNS on the gastric MP and motility

To study the effect of VNS at varying frequencies on gastric MP activity and motility, our study explores a range of frequencies (5, 10, 20, and 30 Hz) commonly employed in both pre-clinical and clinical settings to modulate vagal afferents and efferents for the treatment of various disorders[37]. Despite the widespread use of these frequencies, the differential effects on gastric function remain poorly understood. To investigate this question, we performed in vivo imaging in mice receiving VNS at the above frequencies and closely monitored the activity of gastric myenteric neurons. Before VNS, the MP activity was monitored at rest for approximately 60 seconds. Stimulations were applied in ascending order of frequency, with each frequency applied three times, separated by 30-second intervals between stimulations and approximately 60-second intervals between different frequencies. Our observations revealed frequency-dependent changes in calcium intensity within myenteric neurons, with distinct patterns emerging at each frequency (Fig. 4a–d, see Supplementary Fig. 7 and Supplementary Movie 8). There was a notable increase in ganglionic calcium intensity changes ($\Delta F/F_0$), the percentage of responsive neurons ($\Delta F/F_0 > 50\%$) within each ganglion, and the extent of tissue movement in response to increasing stimulation frequencies (p < 0.0001, $n = 5$ for both $\Delta F/F_0$ and the percentage of responsive neurons, and $p = 0.01$, $n = 3$ for tissue movement). The results are shown in Fig. 4e, indicating changes in $\Delta F/F_0$ at different frequencies (5 Hz: 0.4 ± 0.1, 10 Hz: 0.8 ± 0.3, 20 Hz: 1.2 ± 0.2, 30 Hz: 1.5 ± 0.3). Additionally, Fig. 4f details the percentage of responsive neurons (5 Hz: $38 \pm 9.8\%$, 10 Hz: $55.2 \pm 14.8\%$, 20 Hz: $67.4 \pm 12.4\%$, 30 Hz: $78.0 \pm 9.7\%$), and Fig. 4g depicts the maximal tissue movement observed (5 Hz: 20 ± 10 μm, 10 Hz: 28 ± 7 μm, 20 Hz: 42 ± 8 μm, 30 Hz: 55 ± 13 μm). Furthermore, linear regression analysis revealed a positive correlation between stimulation frequency and changes in calcium intensity ($R^2 = 0.78$), percentage of responsive neurons ($R^2 = 0.57$), and maximum observed tissue movement ($R^2 = 0.66$), as shown in Fig. 4h–j. These results suggest a frequency-dependent enhancement of gastric motility through vagal activation, characterized by increased ganglionic $\Delta F/F_0$ and a greater number of activated myenteric neurons. Importantly, the enhancement of gastric motility was positively correlated with both changes in calcium intensity and the number of activated neurons (Fig. 4k, l), supporting the potential of frequency modulated VNS as a therapeutic strategy to modulate gastric motility.

Effects of VNS and GES on the activity of the same gastric MP

Gastric electrical stimulation (GES) is used clinically to improve symptoms related to impaired gastric motility[38]. GES refers to the electrical stimulation of the surface of the stomach or the vagus nerve branches on the surface of the stomach[39]. To analyze whether VNS differs from GES in enhancing gastric motility, we perform in vivo imaging at the same location to visualize gastric MP activated by VNS and GES, consecutively (Fig. 5a). During our experiments, we found that GES activated almost all neurons and nerve fibers in imaged ganglia when the stimulation frequency reached 10 Hz. Therefore, we opted for a stimulation frequency of 10 Hz for both VNS and GES. Each stimulation was repeated thrice, with VNS preceding GES by approximately 90 seconds. We observed that both VNS and GES stimulated the gastric MP at the same location (Fig. 5b). However, neurons and ganglia activated by VNS showed significantly weaker changes in calcium intensity compared to those activated by GES (Fig. 5c, d and see Supplementary movie 9), and localized tissue movement induced by VNS was less pronounced than that induced by GES (Fig. 5e). We performed this experiment in three mice and found that the risetime of the calcium transient was faster in GES-activated gastric myenteric neurons compared to VNS-activated ones ($p = 0.0131$). (Fig. 5f). Nonetheless, the number of neurons activated by VNS within the same ganglia was noticeably fewer ($p < 0.01$) than that in GES-activated (Fig. 5g). This difference in number may be since VNS activates neurons innervated by the vagus nerve, whereas GES activates not only vagus nerve[40] but also sympathetic nerves and intrinsic nerve fibers[41] (Fig. 5h), which in turn activate more neurons. These results demonstrate the ability of our method to observe in real time the effects of two different stimulation methods on the activity of the same gastrointestinal myenteric plexus in vivo.

The vagus nerve innervation of colonic MP

The vagus nerve's innervation of the GI tract terminates in the colon[42], contributing to approximately 16% of the myenteric ganglia innervation in the descending colon[17]. Despite its established role, the vagus nerve's influence on colonic motility remains a subject of debate. In this study, we replaced the gastric scaffold with an intestinal scaffold for in vivo colonic imaging to investigate the effects of vagal activation on the colonic MP and motility. In particular, the colon is predominantly innervated by the right vagus nerve of the neck[43]. CTB-555 was administered to the proximal colon (5 sites, 400 nL each) to trace the vagus nerve that innervates the colon (Fig. 6a). A limited number of neurons were observed in the right nodose ganglion (Fig. 6b). Therefore, we chose to stimulate the right vagus nerve, facilitating observe myenteric activity in the proximal colon (Fig. 6c). Because of the predominant influence of the right vagus nerve on the sinus node, stimulation of the right vagus nerve decreased heart rate[44]. We found that
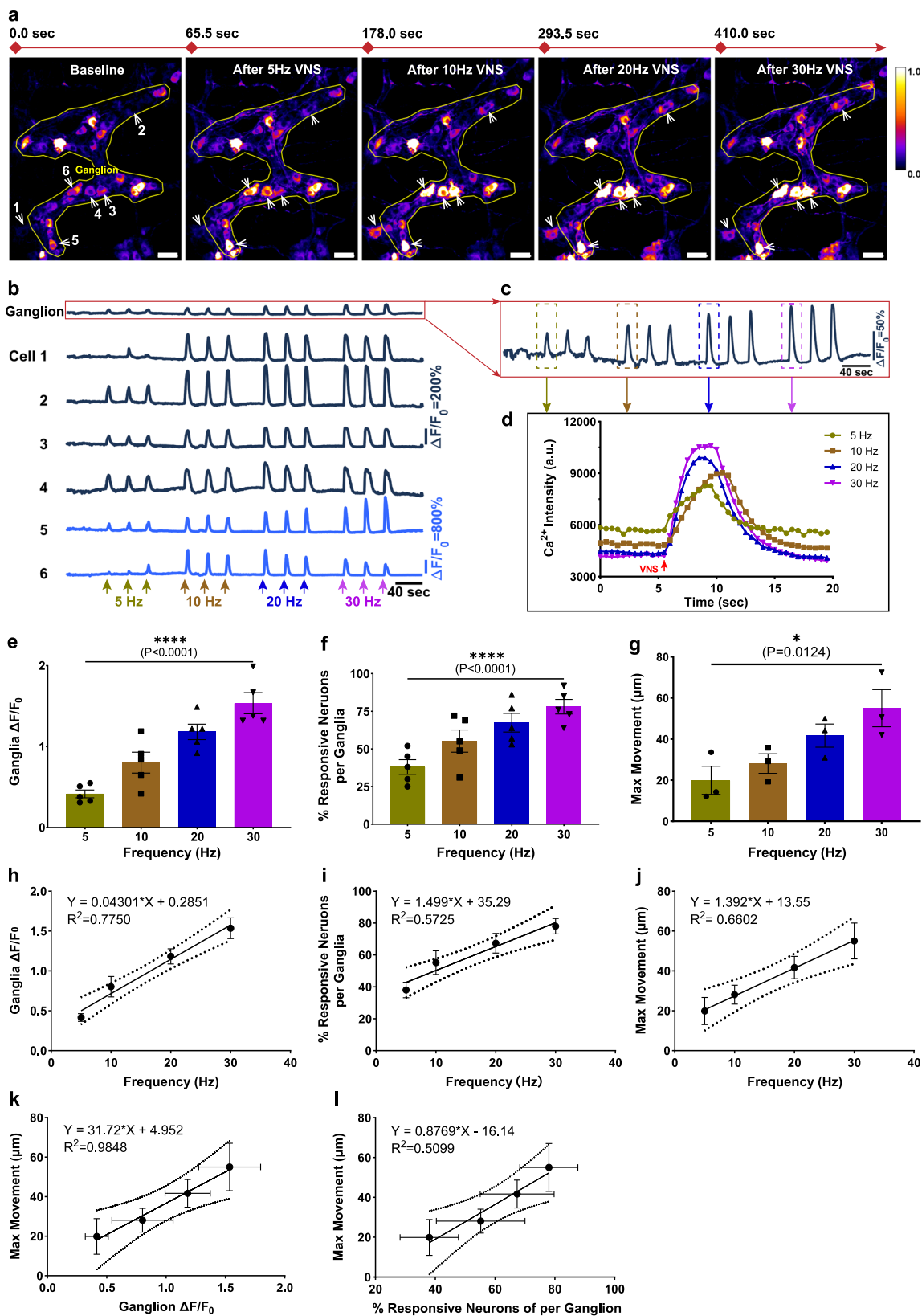
mice died of bradycardia after stimulation at frequencies higher than 15 Hz during our experiments. Therefore, we chose 5, 10, and 15 Hz as the stimulation frequencies. Following stimulation at these frequencies (three repetitions per frequency, with intervals of approximately 30 seconds for the same frequency and 60 seconds between different frequencies), significant changes in calcium intensity were observed in proximal colonic MP ganglia and neurons (ROI) (Fig. 6d, e and see Supplementary Movie 10). However, no significant differences in calcium intensity changes ($\Delta F/F_0$) were found between stimulations (Fig. 6f). In addition, no stimulus-related changes in colonic tissue movement were detected during the nine stimulations (Fig. 6f, h), with the observed tissue movements considered to be spontaneous

Fig. 4 | Response of the gastric MP to VNS at different frequencies.
a Representative images of GCaMP6s-expressing gastric myenteric neurons at 0, 65.5, 178, 293.5, and 410 seconds, both before and after 5, 10, 20, and 30 Hz VNS. All scale bars are 50 μm. **b** Changes in the calcium intensity ($\Delta F/F_0$) from **a** (indicated by a yellow box and white arrows) in response to 5 (olive arrow), 10 (brown arrow), 20 (blue arrow) and 30 (purple arrow) Hz VNS (3 stimulations per frequency). **c** The detail view shows the $\Delta F/F_0$ of the ganglion in **b** after magnification by a factor of 4. **d** Changes in calcium intensity during 20 seconds before and after the first stimulation at 5, 10, 20, and 30 Hz. **e** Amplitude of $\Delta F/F_0$ increased with increasing frequency ($F_{2.1, 8.6} = 50.78$, $p < 0.0001$, n = 5 mice). **f** Percentage of responsive neurons per ganglion increased with increasing frequency ($F_{2.2, 8.9} = 55.21$,

$p < 0.0001$, $n = 5$ mice). **g** Tissue max movement increased with increasing frequency ($F_{1.4, 2.8} = 33.33$, $p = 0.01$, $n = 3$ mice). ns: $p > 0.05$, *$p < 0.05$, ****$p < 0.0001$, RM one-way ANOVA, Tukey post hoc test (**e**–**g**). **h**–**j** Linear regression analysis of the distribution of $\Delta F/F_0$ of the ganglion (**h**), percentage of responsive neurons per ganglion (**i**) and tissue max movement (**j**) under different frequency stimulations. **k, l** Linear regression analysis of the distribution of $\Delta F/F_0$ of the ganglion, and percentage of responsive neurons per ganglion to tissue max movement. X numbers with error values to plot horizontal error bars. **h**–**l** The solid line refers to the linear regression equation. All data are mean ±s.e.m Dashed lines indicate 95% confidence band.

(see Supplementary Fig. 10). Analysis revealed no significant differences in $\Delta F/F_0$ (5 Hz: 1.9 ± 0.9, 10 Hz: 1.8 ± 0.8, 15 Hz: 1.9 ± 0.9, $p = 0.99$, $n = 4$ mice), the percentage of responsive neurons per ganglion (5 Hz: 6.5 ± 2.0 %, 10 Hz: 6.5 ± 2.0 %, 15 Hz: 6.5 ± 2.0 %, $n = 4$ mice) and the max movement of tissue (5 Hz: 2 ± 1 μm, 10 Hz: 2 ± 2 μm, 15 Hz: 5 ± 4 μm, $p = 0.23$, $n = 3$ mice) after VNS at different frequencies (Fig. 6i–l). These results indicate that right VNS activates a minimal number of colonic myenteric neurons (approximately 6%), in stark contrast to its effect on gastric myenteric neurons. Furthermore, the level of activation was not dependent on stimulus frequency, and right VNS did not induce the proximal colonic motility, suggesting that the right vagus nerve has a limited effect on colonic motility due to its limited innervation.

Discussion

In this study, we developed a novel method that enables cell-resolution imaging of the stomach in living mice for the first time. This technique significantly reduces motion artifacts caused by extrinsic movements such as breathing and heartbeat. As a result, it allows more accurate analysis of ENS activity and muscle layer movements. Furthermore, by simply replacing the gastric scaffold with an intestinal scaffold, this method can be adapted for in vivo imaging of the intestine. By injecting rAAV into the GI wall to label the ENS, our study demonstrates that the structure and activity of the MP in the GI tract can be stably imaged in vivo over extended periods of time. We found that the higher the stimulation frequency (5–30 Hz), the greater the number of gastric myenteric neurons activated by VNS, leading to more vigorous movements of gastric muscle tissue and a faster gastric emptying rate. In contrast, VNS activates few colonic myenteric neurons and does not induce colonic tissue movement. There is no significant difference in the response of the colonic MP to stimuli of different frequencies. These results highlight a strong contrast between the effects of VNS on colonic and gastric myenteric neurons, with only a minimal number of colonic myenteric neurons (approximately 6%) being activated.

The ENS is located in the intestinal wall and can autonomously control digestive functions[45]. Structural and functional studies of the ENS in live animals using optical imaging methods have been challenging due to the location and motion of the GI tract[8,13]. A previous study successfully achieved optical recording of the ENS in living mice. This was accomplished by using two distinct implantable windows tailored for the small intestine and colon, respectively[8,13]. Despite these advances, the application of these methods has been predominantly limited to the lower GI tract. In contrast, imaging of the upper GI tract, particularly the stomach, is complicated by obstructions from surrounding tissues such as the sternum and liver, as well as the highly variable volume of the stomach, making in vivo imaging of the gastric ENS particularly challenging. The method we developed overcomes these obstacles and facilitates in vivo imaging of the stomach. This innovation allows, for the first time, prolonged and stable optical recording of gastric ENS activity and tissue motion. Furthermore, we have confirmed that this method can be extended to optical recordings of the small intestine, cecum, and colon using a similar approach.

The ENS consists of two ganglionated plexuses: the myenteric plexus (MP) and the submucosal plexus (SMP), the latter is rarely

found in the stomach[46]. The vagus nerve, as one of the direct bridges between the ENS and the CNS, begins in the brainstem and directly innervates the ENS. It particularly innervates almost 100% of ganglia in the gastric ENS[17]. Additionally, vagal preganglionic efferents interact predominantly with both nNOS+ and nNOS- gastric myenteric neurons[47]. Previous studies have investigated the structural connections between the vagus nerve and the MP using nerve tracers[47–49]. Additionally, they assessed the response of myenteric neurons to vagal activation using Fos as a marker[50–54]. Researchers have also evaluated the effect of stress on colonic motility in awake mice using the non-invasive solid-state manometry method[55] and the effect of VNS on gastric motility using magnetic resonance imaging (MRI)[56]. But little is known about how the real-time activity of myenteric neurons and motility of gastric antrum are affected by the vagus nerve. By comparison, a sampling rate of 2 fps was sufficient for in vivo recording of myenteric neuronal activity[23], and thus we chose a 2 fps sampling rate to obtain better image quality (see supplementary Fig. 4). For prolonged in vivo calcium imaging, we chose the GCaMP6s indicator to obtain a higher signal-to-noise ratio of calcium signals. We recorded the activity of gastric myenteric neurons expressing GCaMP6s through in vivo calcium imaging, following the injection of rAAV into GI wall. Our results show that a large number of gastric myenteric neurons respond to vagal activation, consistent with previous results obtained using electrophysiology and immunohistochemistry in vitro[57,58]. We also observed that vagal activation induces local gastric tissue movement, consistent with previous studies in vivo using MRI techniques that VNS enhances gastric motility[59]. However, our approach found that the response of gastric myenteric neurons and the activity of local gastric tissue occur almost simultaneously and reach a resting state at the same time, suggesting vagal activity activates gastric motor neurons that innervate the smooth muscle layers and regulate motility[4,28]. In addition, the number of activated neurons and maximum movement of gastric tissue increased with the frequency of vagal stimulation (5-30 Hz). This observation highlights the need for further research to resolve the variability observed at different stimulation frequencies. The vagus nerve contains approximately 80% afferent and 20% efferent fibers[2]. Stimulation of the cervical vagus nerve activates both afferent and efferent nerves. However, 2 fps was only able to record all the gastric myenteric neurons activated by the vagus nerve. It was unable to differentiate between activations caused by afferent and efferent nerves. This is because the slow sampling rate cannot determine whether the observed effect is direct or mediated through a reflex pathway following vagus nerve activation. Differences between them can be discriminated later in real time by using the methods we have developed in combination with fast calcium imaging or selective photoactivation of vagal afferents and efferents[60]. Future studies could explore faster sampling rates, the optimization of stimulation parameters, selective stimulation of vagal fibers, and distinct labeling of neurons based on their functional roles to improve our understanding of the vagal influence on gastric motility.

The use of GES as a therapeutic tool is being trialed in an increasing range of human diseases, including gastric motility disorders. It has been reported that GES partially activates almost all
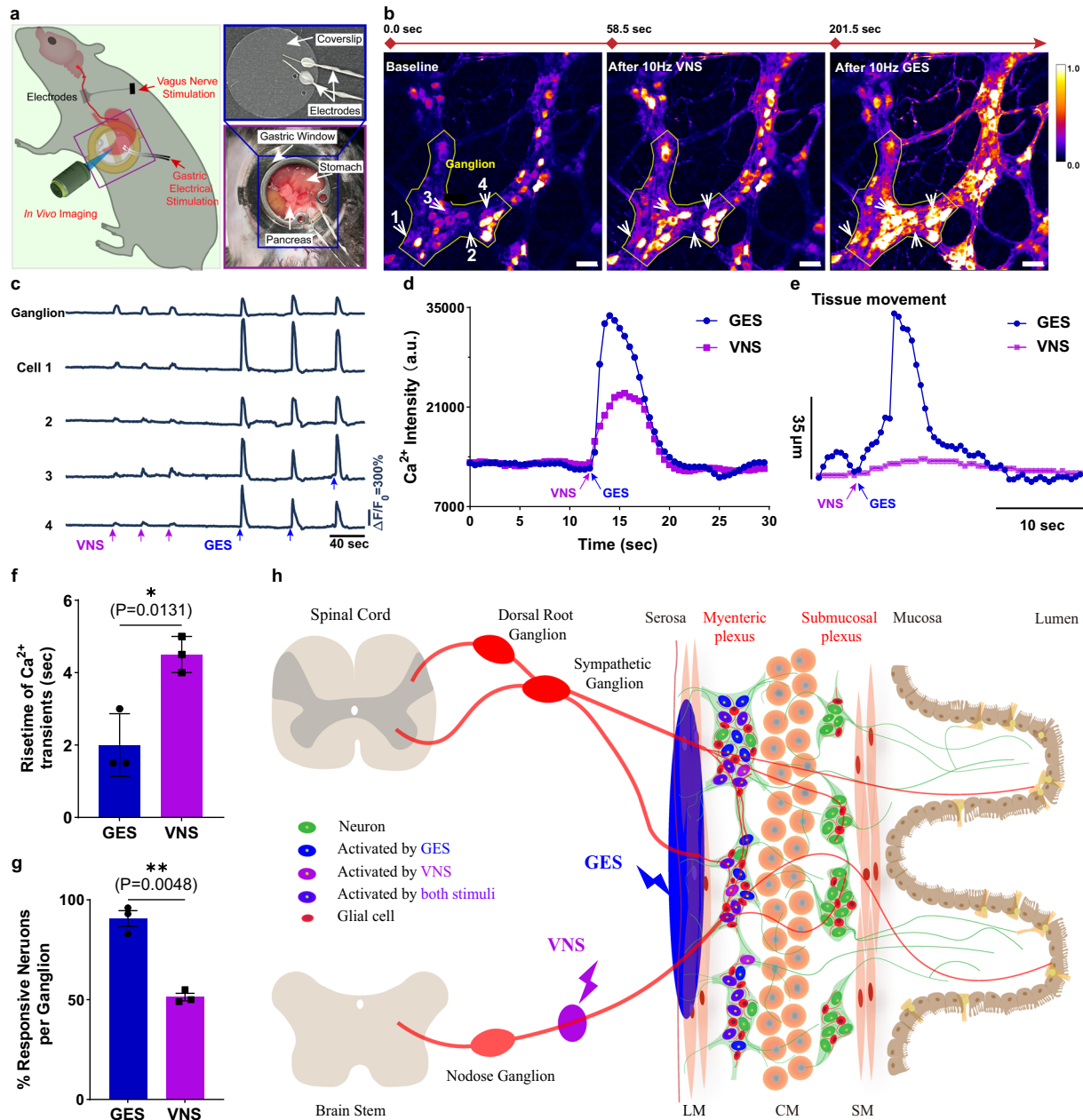
Fig. 5 | Differences in activation of gastric myenteric neurons by VNS and GES. **a** Schematic of the response to VNS and GES by in vivo imaging at the same location of gastric MP. The schematic shows electrode implantation for GES in a detailed view depicted inside a purple box, and the connection of the electrode and coverslip via dental cement illustrated inside a blue box. **b** Acquired images during in vivo confocal imaging: before stimulation, 58.5 seconds after vague nerve stimulation, and 201.5 seconds after gastric electric stimulation. Yellow boxes are ganglion of interest, and white arrows are neurons of interest. All scale bars are 50 µm. **c** Changes in calcium intensity ($\Delta F/F_0$) from **b** ganglion and neurons responds to 10 Hz VNS and GES. Three times for both VNS (purple arrows) and GES (blue arrows). **d** Calcium intensity of ganglion changed during 30 seconds before and after the first stimulation at 10 Hz VNS and GES. **e** Tissue movement of the stomach after GES and VNS. **f** Difference in risetime of calcium transients induced by 10 Hz VNS and GES. ($t_2 = 9$, *$p < 0.5$, $n = 3$ mice). **g** Percentages of responsive neurons per ganglion after 10 Hz VNS and GES. ($t_2 = 14.42$, p = 0.005, $n = 3$ mice). Star indicates a significant difference between VNS and GES. **f, g** paired Student t-test (Two-tailed), *$p < 0.05$, **$p < 0.01$. **h** Schematic representation of the differences between VNS and GES activation of ENS. LM, longitudinal muscle, CM, circular muscle, and SM, submucosal muscle. All data are mean ± s.e.m.

neural elements within the gastric musculature[38], whereas VNS activates the gastric myenteric neurons innervated by vagal fibers[61]. Our method allowed in vivo recordings of the effects of VNS and GES on myenteric neuronal activity and tissue movement in the same mice. We found that, in the area about 1 mm from the gastric stimulation electrode, the changes in calcium intensity, the number of activated neurons, and the movement of tissues were significantly weaker for VNS than for GES. Possible reasons for these differences are that GES produces more action potentials in the activation of myenteric neurons in

the gastric antrum compared to VNS, and that the neural circuit activated by GES and VNS are not the same, activating different numbers of neurons with varying functions (inhibitory and excitatory). The faster risetime of the calcium transient in neurons activated by GES compared to those activated by VNS is likely due to the two stimulation methods having different neuro-modulatory mechanisms or activating different calcium channels. In our study, The location of the MP being recorded was within approximately 1 mm of the electrode, because of the maximum movement of gastric tissue varies with the distance
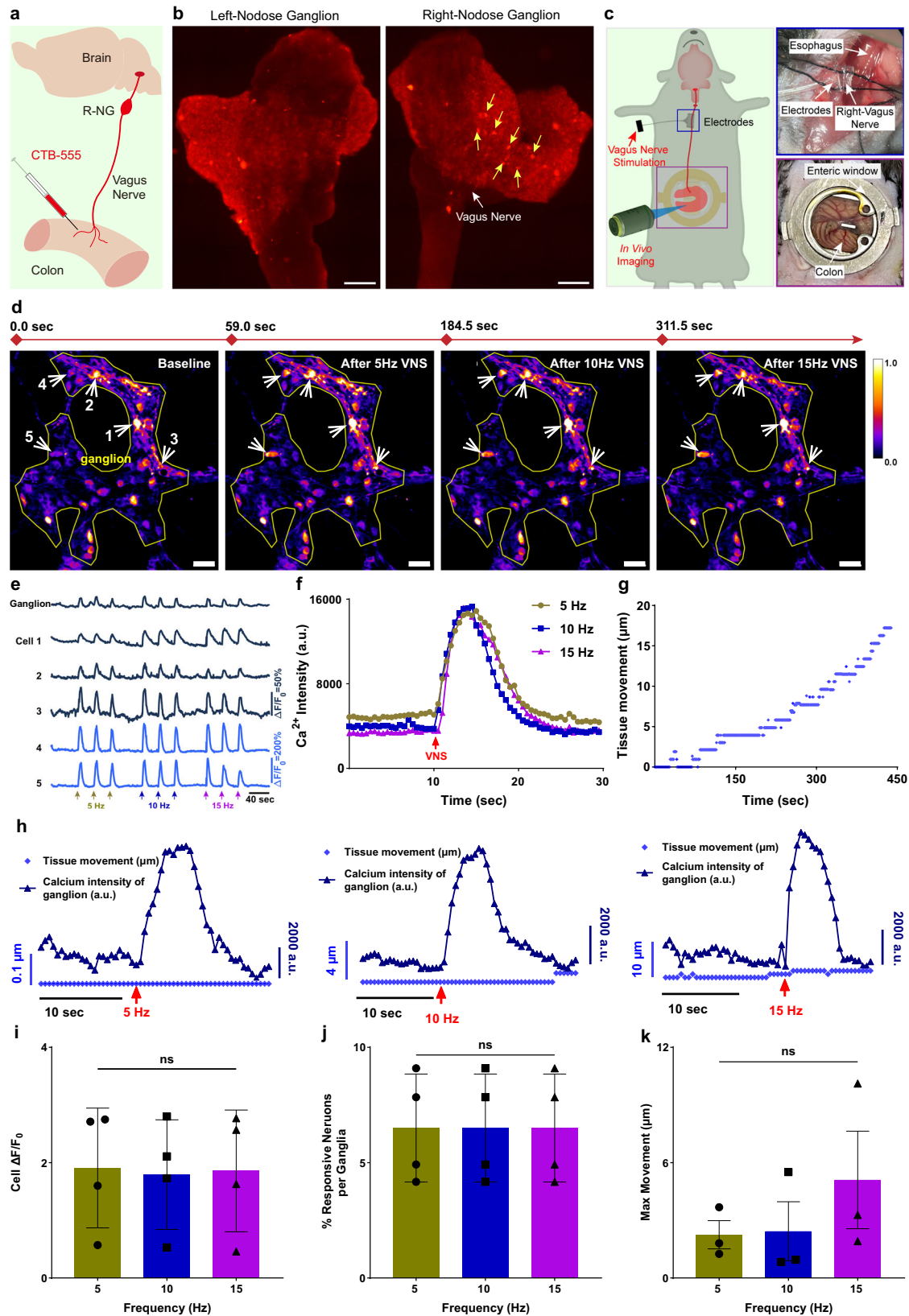
between the recording point and the electrode position on the surface of the stomach. As a result, there are difficulties in quantitatively analyzing the difference between the effects of VNS versus GES on the GI motility.

Vagal innervation of the GI tract terminates within the colon, where the innervation density of colonic neurons is less than 20%[17].

The role of vagal activation in modulating colonic motility remains controversial, underscored by the divergent observations that vagal stimulation elicits different contractile responses in different colonic segments in anesthetized rats[62]. Some studies in anesthetized cats propose that vagal stimulation induces contraction throughout the entire colon[63], while others demonstrate contraction confined to the

Fig. 6 | In vivo calcium imaging of colonic MP in response to VNS. a Cartoon depiction of a strategy for tracing the vagus nerve from the colon. **b** Native fluorescence whole-map analysis of left- and right- ganglion and vagus nerves (white arrow) after colonic infection with CTB-555 in C57BL/6J mice. The yellow arrows point to infected neurons. All scale bars are 200 μm. **c** Schematic of in vivo imaging of mouse colon, the purple box shows a detailed view of the intestinal window after implantation and the blue shows electrode implantation for the right VNS. **d** Frames captured during in vivo confocal imaging of colonic myenteric neurons expressing GCaMP6s at 59, 184.5, and 311.5 seconds after 5, 10, and 15 Hz VNS. All scale bars are 50 μm. **e** Changes in calcium intensity ($\Delta F/F_0$) after VNS at different frequencies in the region of interest (ganglion and neurons) in (**d**). Each of the three different frequencies was stimulated 3 times, with an interval of approximately 30 s between

stimulation at the same frequency and 60 s between stimulation at different frequencies. $\Delta F/F_0 = 200\%$ for the vertical coordinates of cells 4 and 5, and 50% for the others. **f** The calcium intensity of ganglion changed during 30 seconds before and after the first stimulation at 5, 10, and 15 Hz VNS. **g** Changes in colonic tissue movement throughout vagal stimulation. **h** Tissue movement and Ca^{2+} intensity of ganglion changes over a 30-second period before and after 5, 10, and 15 Hz VNS. The red lines refer to tissue movement and the blue refer to calcium intensity of ganglion. **i** The calcium intensity of cells changed ($\Delta F/F_0$) after 5, 10, and 15 Hz VNS ($F_{1.1,\ 3.2} = 0.74$, $p = 0.57$, $n = 4$). **j** Percentages of responsive neurons per ganglion after 5, 10, and 15 Hz VNS did not change ($n = 4$). **(k)** Tissue max movement after 5, 10, and 15 Hz VNS ($F_{1.0,\ 2.0} = 2.9$, $p = 0.23$, $n = 3$). **i–k** *$P < 0.05$, RM one-way ANOVA, Tukey post hoc test, Multiple comparisons. All data are mean ± s.e.m.

mid and distal colon, with the proximal colon remaining unresponsive[64]. A recent study has found that electrical stimulation of the abdominal vagus nerve in anaesthetized pigs enhances the dynamics of the entire colonic region[65]. In our study, we monitored the responses of myenteric neurons in the proximal colon to in vivo vagal stimulation at different frequencies. Upon evaluating local colonic tissue movement, we found that vagal stimulation activated a relatively small subset of neurons in the MP, with a nearly consistent count across different stimulation frequencies. Notably, we did not observe significant colonic movements in response to varying stimulation frequencies (5-15 Hz). Unlike the digestive movements of the stomach, which are mainly controlled by vagovagal reflexes, the colon primarily dependent on the sympathetic and sacral parasympathetic reflexes[5–7]. This differential reliance suggests a broader difference in the functional innervation of the GI tract by the vagus nerve. Whether the above differences between the proximal colon and stomach are related to the activation of vagal afferents and efferents remains to be further investigated. Our findings argue for a deeper exploration of these differences, which may provide new insights into the complex relationship between the vagus nerve and the ENS[5].

In this study, we introduced a novel method capable of stably observing gastric myenteric neuron activity and tissue movement in live mice. This technique extends its application to in vivo imaging of the small intestine, cecum, and colon, thereby overcoming the challenges associated with studying the ENS in vivo and expanding the scope of ENS research across different GI sites. By providing a direct optical window into the gastric MP and colon, our method illuminates the structural dynamics and responses to vagal activation within these regions. Our results reveal a positive correlation between increased gastric motility and both the strength and number of neurons activated by vagal stimulation. Interestingly, while vagal stimulation activates colonic myenteric neurons, it does not induce colonic motility. This distinction demonstrates the potential of our method to explore the influence of the vagus nerve on ENS activity and gastrointestinal motility, deepening our understanding of the complex interplay between the vagus nerve and the ENS. Moreover, our method promises to providing a path for further investigation of the complex gut-brain neural connectivity.

Methods
Experimental animals
All mice were C57BL/6J male, and 2-month-old to 4-month-old mice were used for all experiments. Mice were placed in a temperature-controlled (20 °C) room in 12-hour light-dark cycles, Mouse feeding chow was SPF-F02-003 (SiPeiFu Biotechnology (Beijing)). All animal procedures were approved by the Hubei Provincial Animal Care and Use Committee and followed the experimental guidelines of the Animal Experimentation Ethics Committee of Huazhong University of Science and Technology. At the end of the experimental cycle, all mice were euthanized using cervical dislocation.

Gastrointestinal rAAV and CTB-555 injection
All surgeries were performed under aseptic conditions. We used Avertin (0.625 g Tribromoethanol and 1.25 ml 2-Methyl-2-butanol) at a concentration of 1.25% for general anesthesia, and all animals were injected subcutaneously at a volume of 0.5 ml per 25 g of mouse body weight. The stomach or intestine was accessed through an anterior median incision. The bowel to be injected was pulled out of the abdominal cavity or a sterilized swab was used to move the liver upwards and expose the full extent of the gastric antrum. We injected rAAV five times (200 nL each time and 100 nL/min) in the region of the gastric antrum or intestine (the ileum or colon) through a polished pulled-glass pipette (Pulled Glass 1.14 OD, World Precision Instruments) with an Ultra Micropump controller (World Precision Instruments). After injection, the muscle layer of the abdominal incision is sutured once, then the skin is sutured to close the wound, and the wound is treated with iodophor[29]. This was followed by anti-inflammation via one subcutaneous injection of penicillin sodium. All mice injected with rAAV in the gastrointestinal wall underwent a three-week waiting period before window implantation to allow for full expression of rAAV in the gastrointestinal tract. CTB-555 (1 μg/μl), rAAV-hSyn-EGFP (5.09E + 12 vg/ml), rAAV-GFaABC1D-mCherry (5.00E + 12 vg/ml), rAAV-hSyn-hChR2-EYFP (5.61E + 12 vg/ml), rAAV-CMV-GCaMP6s (5.00E + 12 vg/ml) and rAAV-hSyn-GCaMP6s (5.00E + 12 vg/ml) were expressed by direct injection into the GI wall. The CTB-555 was used for retrograde tracing of the VN. rAAV-hSyn-EGFP and rAAV-GFaABC1D-mCherry were used for labeling the structure of neurons and glial cells in the ENS, respectively. rAAV-hSyn-hChR2-EYFP was used for exploring the delivery of light-sensitive proteins in the ENS. rAAV-CMV-GCaMP6s and rAAV-hSyn-GCaMP6s were used to label Ca^{2+} in enteric neurons. rAAV-CMV-EGFP (5.00E + 12 vg/ml) was administered via tail vein injection, with each mouse receiving a dose of 200 microliters[20], also waited 3 weeks for expression.

Surgical procedure for gastric window implantation
The abdominal hair of the mice was removed using depilatory cream before surgery. The depilated areas were then disinfected using sterilized alcohol (70%) and povidone-iodine solution (1%). During surgery mice were anesthetized using isoflurane (4% induction, 2% maintenance), eyes were kept moist using eye ointment, and body temperature was maintained at 37 °C using a heating pad. The mice were then placed on their left side and the stomach was exposed by cutting approximately 3 mm in diameter with surgical scissors near the stomach (covered by the liver and ribs). A loop (purse-string) was incised using a medical suture to set the skin and muscle tissue into the second slot of the gastric window, and the suture was tightened and knotted to secure the window. The gastric scaffold is placed into the abdominal cavity through the window, and after guiding the scaffold through the bottom of the gastric sinus using pointed forceps (top view), the scaffold is rotated to support the stomach through the third slot

by aligning the scaffold with the two "ears" of the gastric window. The coverslip and C-ring were then placed into the first slot one at a time (Supplementary Movie 3). Povidone-iodine is applied around the wound, and anti-inflammatory drugs and painkillers are injected subcutaneously. Mice were released from anesthesia. Window implantation of the intestine was performed in the same steps as for window implantation except that the surgical location was in the mid-abdominal region (Supplementary Movie 3). Daily intraperitoneal injections of anti-inflammatory drugs (two days in total).

Vagus nerve stimulation (VNS) and Gastric electrical stimulation (GES)

Mice were anaesthetized with 4% isoflurane for induction and maintained at 1.5% during surgery and stimulation. Eye ointment was applied to the eyes to reduce dryness. Throughout the surgery, the body temperature of the mice was maintained at 37 $^\circ$C using a heating pad. The right or left cervical vagus nerve was exposed through a midline incision in the neck. The vagal trunk was then carefully dissected from the carotid sheath under a stereomicroscope and a cuff electrode (KD-cuff, Kedou BC) was wrapped around the nerve. To stimulate the vagus nerve, the electrode was connected to both a stimulation isolator (Exiso, DL Naturegene Life Sciences) and a pulse generator (Model). VNS was performed using a pulse wave with parameters of 5-30 Hz, 15 V, and 500 μs duration for 5 seconds. Before conducting the GES experiments, we prepared the coverslips. First, we drilled holes (0.8 mm in diameter) in the coverslips. Then, we inserted two platinum wires, each 0.5 mm in diameter, through these holes. The ends of the wires that contact the gastric surface were positioned about 3 mm apart. Finally, we used a UV-cured adhesive to secure the wires in the slits of the holes on the coverslips (see Fig. 5a). The cover slips with electrodes were replaced before GES, and the stimulation method was the same as that of VNS.

In vivo confocal imaging

The dual-channel confocal imaging system built was an orthogonal imaging system. The excitation light was 488 nm and 561 nm (OBIS, 50 mW), and the output power of the objective lens was approximately 1 mW. Scanning (512 pixels * 512 pixels) was performed using XY Galvanometer Sets (Cambridge Technology). Cells were observed in vivo using a 20x, water, NA = 0.5 objective (Nikon). 50 μm pinhole (Thorlabs) was used to filter non-focal signals, and PMT (R3896, Hamamatsu) was used to collect excited fluorescence signals. Z-axis scanning was performed using a Microscope Objective Nanopositioning System (Edmund Optics) (scanning range of 100 μm in 1 μm steps). The samples were positioned using a displacement stage (M-562F-XYZ, Newport). Images were acquired using an acquisition rate of 2 fps, and the images were captured as 16-bit grayscale maps. During imaging, mice were placed on a heating pad to maintain a body temperature of 37 °C, and anesthesia was maintained using isoflurane (4% induction, 1.5-2% maintenance). The window was held in place using a fixation device to minimize motion artifacts during the imaging process. To quantitatively analyze the suppression of motion artifacts during imaging and facilitate rapid localization of the same spot during prolonged imaging, we injected 0.1 ml of TRITC-Dextran (5 mg/ml, Sigma) into the tail vein to label the blood vessels. Each mouse was imaged only once per day and every other day, allowing it to recover for one day.

Gastric emptying rate test

The rate of gastric emptying in mice was tested using a semi-nutritional solid paste. This paste was prepared by dissolving 2.4 g of sodium carboxymethyl cellulose (CMC-Na) in 50 mL of distilled water. Then, 3.2 g of milk powder, 1.6 g of sugar, and 1.6 g of water-soluble starch were added. The mixture was formulated into a semi-solid paste and

refrigerated. It was removed from the refrigerator 2 hours prior to use to allow it to return to room temperature. The mice were fasted and dehydrated for 14 hours before the experiment. Each mouse was gavaged 0.2 ml per 10 g of body weight and waited for 5 minutes after gavage. This was followed by induction anesthesia using isoflurane at a concentration of 4% and continuous anesthesia at a concentration of 1.5%. Electrode implantation (left vagus nerve) and the procedure time was controlled to 15 minutes. The vagus nerve stimulation was performed using a pulse wave with parameters of 20 and 30 Hz, 15 V, and 500 μs duration for 30 seconds. Each stimulation session was followed by a 60-second pause, and the total duration of stimulation was 30 minutes. At the end of stimulation, the electrodes were removed, and the mice were euthanized after waiting 30 minutes (awake state) to remove the stomach. The stomachs of mice were removed by ligating the cardia and pylorus with a thin wire, and cutting the esophagus and duodenum close to the ligated wire. The stomach was weighed on a balance, then the wall of the stomach was cut open, the stomach contents were washed with PBS solution, the water was blotted out with filter paper, and the net weight of the stomach was weighed again. Gastric emptying rat = 1 − [weight of semi-solid paste - (total weight of stomach - net weight of stomach)]/weight of semi-solid paste × 100%.

Imaging data analysis

Optical data were processed in ImageJ software. Image jitter was removed using the plugins Image Stabilizer and Template Matching in ImageJ. The neuronal region of interest (ROI) was manually selected and the mean gray value was calculated for the ROI region. The mean gray value was proportional to the amount of GCaMP fluorescence and was used to determine the relative level of activity during the optical recording. The output files corresponding to the ROIs were stored as an xlsx file. Then import the data into MATLAB (R2022a) for further processing. All data were normalized using the following function: $\Delta F/F_0 = (F − F_0)/F_0$. Fluorescence intensity (F) is the mean gray value of each neuronal ROI. F_0 is the fluorescence signal in the baseline period and was determined by calculating the average of fluorescence signals in the 20 seconds before the start of the stimulus. $\Delta F/F_0$ curves were detrended to eliminate effects such as limit drift caused by photobleaching. Tissue movement in response to VNS and GES was determined using a Template Matching (Align Slices in Stack) in ImageJ, which quantifies the ganglion movement along the x- and y- axes, representing the circular and longitudinal muscles, respectively. The profile of tissue movement is obtained by calculating the change in the axial coordinates of the ganglion in the acquired sequence images. In vitro imaging of nodose ganglion was performed using a Nikon Ni-E microscope (10x objective, NA = 0.4, air). 2 fps vs 20 fps difference analysis was performed using an Olympus BX51WI microscope (20x objective, NA = 1.0, water), and image acquisition was performed using a CMOS camera (C13440-20CU, Hamamatsu).

Statistical analysis

All summary data are presented as means ± s.e.m. Data for different frequencies of stimulation were obtained on the same ganglion of the same mouse. Differences in gastric emptying rate (%) evoked by VNS were compared by the unpaired Student t-test (two-tailed). Differences in responses to different frequency stimuli were compared by RM one-way ANOVA with Tukey post hoc test for multiple comparisons. Differences in responses to VNS and GES were compared by the paired Student t-test (two-tailed). Differences between 2 fps and 20 fps acquisition rates in acquiring activity of gastric neurons activated by the GES were compared by the paired Student t-test (two-tailed). Significance was defined as $p < 0.05$. ns means no statistical difference. All statistical analyzes were performed using GraphPad Prism 9.

Statistics and Reproducibility

The experiments on the effectiveness of the optical window in correcting motion artifacts were repeated five times (Fig. 1h and Supplementary Fig. 7). Experiments for in vivo optical recordings of the stomach were repeated over 30 times (Fig. 1i), over 10 times for recordings of the small intestine (Fig. 1j), and over 30 times for recordings of the proximal colon (Fig. 1k). Prolonged optical recordings of the structure of the gastric MP were repeated three times (Fig. 2a–d), and prolonged optical recordings of calcium activity in gastric myenteric neurons were repeated three times (Fig. 2e, f). Retrograde tracing experiments from the stomach (Fig. 3d) and proximal colon (Fig. 6b) to the nodose ganglia were repeated five times each. In vivo recordings of the response of the gastric MP and the proximal colonic MP to vagal activation were repeated five times (Fig. 3f) and four times (Fig. 6d), respectively. Experiments activating the same gastric MP by gastric electrical stimulation and vagal stimulation were repeated three times. All experiments used different mice for each repetition.

Reporting summary

Further information on research design is available in the Nature Portfolio Reporting Summary linked to this article.

Data availability

The authors declare that the data supporting the findings of this study are available within the paper and its supplementary information files. The data in Fig. 2e, f; Fig. 3b, g–j; Fig. 4b, d–g; Fig. 5c–g; Fig. 6e–k; Supplementary Fig. 4b–g; Supplementary Fig. 6b; Supplementary Fig. 7b; Supplementary Fig. 8b, d; Supplementary Fig. 10b, c, e, f. have associated source data. Source data are provided as a Source Data file. The Source Data generated in this study have been deposited in the Science Data Bank under accession code https://doi.org/10.57760/sciencedb.08864, https://www.scidb.cn/s/ji6bau. Source data are provided with this paper.

Code availability

The authors declare that the custom code used for calcium signal data processing and analysis in this study is available in the Science Data Bank repository[66] https://www.scidb.cn/s/7JJni2, https://doi.org/10.57760/sciencedb.08902. The data in Fig. 2e, f; Fig. 3g; Fig. 4b; Fig. 5c; Fig. 6e and Supplementary Fig. 10b, e have associated custom code.

References

1. Furness, J. B. The enteric nervous system and neurogastroenterology. *Nat. Rev. Gastroenterol. Hepatol.* **9**, 286–294 (2012).
2. Spencer, N. J. & Hu, H. Enteric nervous system: sensory transduction, neural circuits and gastrointestinal motility. *Nat. Rev. Gastroenterol. Hepatol.* **17**, 338–351 (2020).
3. Taché, Y., Garrick, T. & Raybould, H. Central nervous system action of peptides to influence gastrointestinal motor function. *Gastroenterology* **98**, 517–528 (1990).
4. Berthoud, H., Carlson, N. R. & Powley, T. L. Topography of efferent vagal innervation of the rat gastrointestinal tract. *Am. J. Physiol. -Regulatory, Integr. Comp. Physiol.* **260**, R200–R207 (1991).
5. De Groat, W. C. & Krier, J. The sacral parasympathetic reflex pathway regulating colonic motility and defaecation in the cat. *J. Physiol.* **276**, 481–500 (1978).
6. Ridolfi, T. J., Tong, W. D., Takahashi, T., Kosinski, L. & Ludwig, K. A. Sympathetic and parasympathetic regulation of rectal motility in rats. *J. Gastrointest. Surg.* **13**, 2027–2033 (2009).
7. Hedlund, H., Fändriks, L., Delbro, D. & Fasth, S. On the transmission of sacral parasympathetic nervous influence on distal colonic and rectal motility in the cat. *Acta physiologica scandinavica* **125**, 225–234 (1985).
8. Rakhilin, N. et al. Simultaneous optical and electrical in vivo analysis of the enteric nervous system. *Nat. Commun.* **7**, 11800 (2016).
9. Giampetraglia, M. & Weigelin, B. Recent advances in intravital microscopy for preclinical research. *Curr. Opin. Chem. Biol.* **63**, 200–208 (2021).
10. Jacquemin, G. et al. Longitudinal high-resolution imaging through a flexible intravital imaging window. *Sci. Adv.* **7**, eabg7663 (2021).
11. De Niz, M., Nacer, A. & Frischknecht, F. Intravital microscopy: imaging host–parasite interactions in the brain. *Cell. Microbiol.* **21**, e13024 (2019).
12. Chen, C. et al. Long-term imaging of dorsal root ganglia in awake behaving mice. *Nat. Commun.* **10**, 3087 (2019).
13. Rakhilin, N. et al. An intravital window to image the colon in real time. *Nat. Commun.* **10**, 5647 (2019).
14. Entenberg, D. et al. A permanent window for the murine lung enables high-resolution imaging of cancer metastasis. *Nat. methods* **15**, 73–80 (2018).
15. Ritsma, L. et al. Intravital microscopy through an abdominal imaging window reveals a pre-micrometastasis stage during liver metastasis. *Sci. Transl. Med* **4**, 158ra145 (2012).
16. Huang, Q. et al. Intravital imaging of mouse embryos. *Science* **368**, 181–186 (2020).
17. Chang, H. Y., Mashimo, H. & Goyal, R. K. IV. Current concepts of vagal efferent projections to the gut. *Am. J. Physiol. -Gastrointest. Liver Physiol.* **284**, G357–G366 (2003).
18. Vdoviaková, K. et al. Surgical anatomy of the gastrointestinal tract and its vasculature in the laboratory rat. *Gastroenterology res. prac.* **2016**, 2632368 (2016).
19. CHANG, F. Y. Electrogastrography: basic knowledge, recording, processing and its clinical applications. *J. Gastroenterol. Hepatol.* **20**, 502–516 (2005).
20. Chan, K. Y. et al. Engineered AAVs for efficient noninvasive gene delivery to the central and peripheral nervous systems. *Nat. Neurosci.* **20**, 1172–1179 (2017).
21. Tang, Y. et al. In vivo two-photon calcium imaging in dendrites of rabies virus-labeled v1 corticothalamic neurons. *Neurosci. Bull.* **36**, 545–553 (2020).
22. Motegi, Y. et al. Confocal and multiphoton calcium imaging of the enteric nervous system in anesthetized mice. *Neurosci. Res* **151**, 53–60 (2020).
23. Obata, Y. et al. Neuronal programming by microbiota regulates intestinal physiology. *Nature* **578**, 284–289 (2020).
24. Fried, D. E. & Gulbransen, B. D. In situ Ca^{2+} imaging of the enteric nervous system. *J. Vis. Exp.* https://doi.org/10.3791/52506 (2015).
25. Goto, K. et al. In vivo imaging of enteric neurogenesis in the deep tissue of mouse small intestine. *PLoS One* **8**, e54814 (2013).
26. Gulbransen, B. D. & Sharkey, K. A. Purinergic neuron-to-glia signaling in the enteric nervous system. *Gastroenterology* **136**, 1349–1358 (2009).
27. Dai, S. et al. In situ generation of red-to-NIR emissive radical cations in the stomach for gastrointestinal imaging. *Adv. Mater.* **35**, e2209940 (2023).
28. Berthoud, H. R., Jedrzejewska, A. & Powley, T. L. Simultaneous labeling of vagal innervation of the gut and afferent projections from the visceral forebrain with dil injected into the dorsal vagal complex in the rat. *J. Comp. Neurol.* **301**, 65–79 (1990).
29. Ritsma, L. et al. Surgical implantation of an abdominal imaging window for intravital microscopy. *Nat. Protoc.* **8**, 583–594 (2013).
30. Travagli, R. A. & Anselmi, L. Vagal neurocircuitry and its influence on gastric motility. *Nat. Rev. Gastroenterol. Hepatol.* **13**, 389–401 (2016).
31. Chambers, A. P. et al. Regulation of gastric emptying rate and its role in nutrient-induced GLP-1 secretion in rats after vertical sleeve gastrectomy. *Am. J. Physiol. -Endocrinol. Metab.* **306**, E424–E432 (2014).

32. Hirota, R., Okano, H. & Hisa, Y. *Nodose Ganglion*. *Neuroanatomy and Neurophysiology of the Larynx*, 73–82 (2016).

33. Muller, P. A. et al. Microbiota modulate sympathetic neurons via a gut-brain circuit. *Nature* **583**, 441–446 (2020).

34. Bowles, S. et al. Vagus nerve stimulation drives selective circuit modulation through cholinergic reinforcement. *Neuron* **110**, 2867–2885. e2867 (2022).

35. Val-Laillet, D., Biraben, A., Randuineau, G. & Malbert, C. H. Chronic vagus nerve stimulation decreased weight gain, food consumption and sweet craving in adult obese minipigs. *Appetite* **55**, 245–252 (2010).

36. Smith-Edwards, K. M. et al. Extrinsic primary afferent neurons link visceral pain to colon motility through a spinal reflex in mice. *Gastroenterology* **157**, 522–536 e522 (2019).

37. Bonaz, B., Sinniger, V. & Pellissier, S. Anti-inflammatory properties of the vagus nerve: potential therapeutic implications of vagus nerve stimulation. *J. Physiol*. **594**, 5781–5790 (2016).

38. Payne, S. C., Furness, J. B. & Stebbing, M. J. Bioelectric neuromodulation for gastrointestinal disorders: effectiveness and mechanisms. *Nat. Rev. Gastroenterol. Hepatol*. **16**, 89–105 (2019).

39. Liu, J., Qiao, X. & Chen, J. Vagal afferent is involved in short-pulse gastric electrical stimulation in rats. *Digestive Dis. Sci*. **49**, 729–737 (2004).

40. Qin, C., Sun, Y., Chen, J. & Foreman, R. D. Gastric electrical stimulation modulates neuronal activity in nucleus tractus solitarii in rats. *Autonomic Neurosci*. **119**, 1–8 (2005).

41. Barth, B. B., Travis, L., Spencer, N. J. & Grill, W. M. Control of colonic motility using electrical stimulation to modulate enteric neural activity. *Am. J. Physiol. -Gastrointest. Liver Physiol*. **320**, G675–G687 (2021).

42. Stakenborg, N., Di Giovangiulio, M., Boeckxstaens, G. E. & Matteoli, G. The versatile role of the vagus nerve in the gastrointestinal tract. *Eur. Med. J. Gastroenterol*. **1**, 106–114 (2013).

43. Altschuler, S. M., Escardo, J., Lynn, R. B. & Miselis, R. R. The central organization of the vagus nerve innervating the colon of the rat. *Gastroenterology* **104**, 502–509 (1993).

44. Ng, G. A., Brack, K. E. & Coote, J. H. Effects of direct sympathetic and vagus nerve stimulation on the physiology of the whole heart–a novel model of isolated Langendorff perfused rabbit heart with intact dual autonomic innervation. *Exp. Physiol*. **86**, 319–329 (2001).

45. Niesler, B., Kuerten, S., Demir, I. E. & Schafer, K. H. Disorders of the enteric nervous system - a holistic view. *Nat. Rev. Gastroenterol. Hepatol*. **18**, 393–410 (2021).

46. Furness, J. B. *The Enteric Nervous System*. (John Wiley & Sons, 2008).

47. Jaffey, D. M., McAdams, J. L., Baronowsky, E. A., Black, D. & Powley, T. L. Vagal preganglionic axons arborize in the myenteric plexus into two types: nitrergic and non-nitrergic postganglionic motor pools? *Am. J. Physiol. Regul. Integr. Comp. Physiol*. **324**, R305–r316 (2023).

48. Powley, T. L. Vagal input to the enteric nervous system. *Gut* **47**, iv30–iv32 (2000).

49. Hayakawa, T., Kuwahara, S., Maeda, S., Tanaka, K. & Seki, M. Direct synaptic contacts on the myenteric ganglia of the rat stomach from the dorsal motor nucleus of the vagus. *J. Comp. Neurol*. **498**, 352–362 (2006).

50. Berthoud, H. R., Patterson, L. M. & Zheng, H. Vagal-enteric interface: vagal activation-induced expression of c-Fos and p-CREB in neurons of the upper gastrointestinal tract and pancreas. *Anat. Rec*. **262**, 29–40 (2001).

51. Yuan, P. Q., Wu, S. V., Wang, L. & Taché, Y. The ghrelin agonist, HM01 activates central vagal and enteric cholinergic neurons and reverses gastric inflammatory and ileus responses in rats. *Neurogastroenterol. Motil*. **35**, e14561 (2023).

52. Yuan, P. Q. et al. Central vagal stimulation activates enteric cholinergic neurons in the stomach and VIP neurons in the duodenum in conscious rats. *Peptides* **26**, 653–664 (2005).

53. Zheng, H. & Berthoud, H.-R. Functional vagal input to gastric myenteric plexus as assessed by vagal stimulation-induced Fos expression. *Am. J. Physiol. -Gastrointest. Liver Physiol*. **279**, G73–G81 (2000).

54. Miampamba, M., Yang, H., Sharkey, K. A. & Taché, Y. Intracisternal TRH analog induces Fos expression in gastric myenteric neurons and glia in conscious rats. *Am. J. Physiol. -Gastrointest. Liver Physiol*. **280**, G979–G991 (2001).

55. Gourcerol, G. et al. Cholinergic giant migrating contractions in conscious mouse colon assessed by using a novel noninvasive solid-state manometry method: modulation by stressors. *Am. J. Physiol. Gastrointest. Liver Physiol*. **296**, G992–g1002 (2009).

56. Lu, K. H., Cao, J., Phillips, R., Powley, T. L. & Liu, Z. Acute effects of vagus nerve stimulation parameters on gastric motility assessed with magnetic resonance imaging. *Neurogastroenterol. Motil*. **32**, e13853 (2020).

57. Schemann, M. & Grundy, D. Electrophysiological identification of vagally innervated enteric neurons in guinea pig stomach. *Am. J. Physiol. -Gastrointest. Liver Physiol*. **263**, G709–G718 (1992).

58. Furness, J. B., Callaghan, B. P., Rivera, L. R. & Cho, H.-J. The enteric nervous system and gastrointestinal innervation: integrated local and central control. *Microbial endocrinology: The microbiota-gut-brain axis in health and disease*, 39-71 (2014).

59. Lu, K. H. et al. Vagus nerve stimulation promotes gastric emptying by increasing pyloric opening measured with magnetic resonance imaging. *Neurogastroenterol. Motil*. **30**, e13380 (2018).

60. Okonogi, T. & Sasaki, T. *Optogenetic Manipulation Of The Vagus Nerve*. *Optogenetics: Light-Sensing Proteins and Their Applications in Neuroscience and Beyond*,**1293**, 459-470 (2021).

61. de Lartigue, G. Role of the vagus nerve in the development and treatment of diet-induced obesity. *J. Physiol*. **594**, 5791–5815 (2016).

62. Tong, W. D., Ridolfi, T. J., Kosinski, L., Ludwig, K. & Takahashi, T. Effects of autonomic nerve stimulation on colorectal motility in rats. *Neurogastroenterol. Motil*. **22**, 688–693 (2010).

63. Rostad, H. Colonic motility in the cat: II. extrinsic nervous control. *Acta Physiologica Scandinavica* **89**, 91–103 (1973).

64. Hultén, L. & Jodal, M. Extrinsic nervous control of colonic motility and blood flow: an experimental study in the cat. **335**, 1–116 (1969).

65. Larauche, M. et al. The effect of colonic tissue electrical stimulation and celiac branch of the abdominal vagus nerve neuromodulation on colonic motility in anesthetized pigs. *Neurogastroenterol. Motil*. **32**, e13925 (2020).

66. Longjie, J. et al. In vivo imaging of vagal-induced myenteric plexus responses in gastrointestinal tract with an optical window. Science Data Bank https://doi.org/10.57760/sciencedb.08902 (2024).

Acknowledgements

Author contributions

L.F. and L.J. designed the study. L.J. designed the experiments. L.J. and J.Y. finished the experiments and analyzed the data. L.J. wrote the manuscript. L.J., J.Y., X.G., and L.F. edited the manuscript. J.H. assisted in the construction of the confocal imaging system. L.F. and Q.L. acquired funding for the project.

Competing interests

The authors declare no competing interests.

Additional information